

1 **Title: Revealing the cell-material interface with nanometer resolution by**  
2 **FIB-SEM**

3 **Authors:** Francesca Santoro<sup>1\*</sup>, Wenting Zhao<sup>1,2</sup>, Lydia-Marie Joubert<sup>3</sup>, Liting Duan<sup>1</sup>, Jan  
4 Schnitker<sup>4</sup>, Yoeri van de Burgt<sup>2</sup>, Hsin-Ya Lou<sup>1</sup>, Bofei Liu<sup>2</sup>, Alberto Salleo<sup>2</sup>, Lifeng Cui<sup>5</sup>, Yi  
5 Cui<sup>2,6</sup>, Bianxiao Cui<sup>1\*</sup>

6 **Affiliations:**

7 <sup>1</sup> Department of Chemistry, Stanford University, Stanford, CA94305, USA

8 <sup>2</sup>Department of Material Science and Engineering, Stanford University, Stanford,  
9 CA94305, USA

10 <sup>3</sup>CSIF Beckman Center, Stanford University, Stanford, 94305, USA

11 <sup>4</sup>Institute of Bioelectronics ICS/PGI-8, Forschungszentrum Juelich, Juelich, 52428,  
12 Germany

13 <sup>5</sup>Department of Material Science and Engineering, Dongguan University of Technology,  
14 Guangdong 523808, China

15 <sup>6</sup>Stanford Institute for Materials and Energy Sciences, SLAC National Accelerator, Menlo  
16 Park, CA94025, USA

17

18 *\*Correspondence to: bcui@stanford.edu, santorof@stanford.edu*

19 **The interface between biological cells and non-biological surfaces profoundly influences**  
20 **cellular activities, chronic tissue responses, and ultimately the success of medical**  
21 **implants. Materials in contact with cells can be plastics, metal, ceramics or other synthetic**  
22 **materials, and their surfaces vary widely in chemical compositions, stiffness, topography**  
23 **and levels of roughness. To understand the molecular mechanism of how cells and tissues**  
24 **respond to different materials, it is of critical importance to directly visualize the cell-**  
25 **material interface at the relevant length scale of nanometers. Conventional ultrastructural**  
26 **analysis by transmission electron microscopy (TEM) often requires substrate removal**  
27 **before microtome sectioning, which is not only challenging for most substrates but also**  
28 **can cause structural distortions of the interface. Here, we present a new method for *in situ***  
29 **examination of the cell-to-material interface at any desired cellular location, based on**  
30 **focused-ion beam milling and scanning electron microscopy imaging (FIB-SEM). This**  
31 **method involves a thin-layer plastification procedure that preserves adherent cells as well**

32 **as enhances the contrast of biological specimen. We demonstrate that this unique**  
33 **procedure allows the visualization of cell-to-material interface and intracellular structures**  
34 **with 10nm resolution, compatible with a variety of materials and surface topographies, and**  
35 **capable of volume and multi-directional imaging. We expect that this method will be very**  
36 **useful for studies of cell-to-material interactions and also suitable for *in vivo* studies such**  
37 **as examining osteoblast adhesion and new bone formation in response to titanium**  
38 **implants.**

39

40 Many biological applications and biomedical devices require direct contact between biological  
41 cells and non-biological materials<sup>1</sup>. In the case of medical implants, the cell-to-material interface  
42 is a key determinant for successful device integration with surrounding tissues, providing  
43 mechanical support and minimizing host foreign body responses<sup>2</sup>. In addition to providing  
44 mechanical support, non-biological materials are actively explored for inducing the regeneration  
45 and repair of surrounding tissues<sup>2</sup>. In this context, the cell-to-material interface is essential in  
46 regulating cell signaling, guiding cell migration, and controlling stem cell differentiation and lineage  
47 specificity<sup>3,4</sup>.

48 To date, ultrastructural analysis by transmission electron microscopy (TEM) is the most detailed  
49 method for analyzing the cell-to-material interface. TEM can resolve the cell membrane and  
50 subcellular structures, which reveals how cells make contacts with the substrate surface and  
51 provides accurate measurement of the gap distance between the cell membrane and the material  
52 surface<sup>5-7</sup>. However, the TEM method requires embedding the sample in millimeter-sized resin  
53 blocks and, then, sectioning them into ultra-thin slices (~100 nm thickness) with mechanical  
54 knives. In many cases (*i.e.* hard materials such as glass and metals), the substrate has to be  
55 removed by chemical etching or physical separation before sectioning. Substrate removal is often  
56 not feasible for many systems, and even if feasible, the procedure can induce structural artifacts  
57 at the interface. Furthermore, in TEM resin-blocks, the context of the cell is lost unless a 3D  
58 reconstruction is carried out after a tedious procedure of sectioning, sorting and imaging hundreds  
59 of individual slices.

60 A combination of focused ion beam (FIB) and scanning electron microscopy (SEM) constitutes  
61 an alternative approach for sectioning/imaging of materials<sup>8</sup> and biological specimens<sup>9</sup>. Unlike  
62 TEM, FIB-SEM allows *in situ* ion-based milling of the specimen to reveal interfaces at any desired  
63 location. The use of FIB-SEM for examining the interaction of cells with engineered surfaces has  
64 been previously explored by us<sup>10,11</sup> and by others<sup>12-17</sup>. However, using FIB-SEM for cell-to-  
65 material interface studies is severely limited by structural damages and the poor contrast of the

66 biological specimen, usually prepared by hard drying procedures. The drying procedure can  
67 induce substantial volume shrinkage<sup>18,19</sup>, as well as cavities (sponge-like morphology) in place of  
68 the intracellular compartments<sup>14,16</sup>. The lack of contrast in biological specimens results in an  
69 inability to resolve the intracellular structures or the cell membrane. Recently, a thin-layer resin  
70 embedding method has been developed<sup>16,20</sup>, but the lack of contrast (*i.e.* no heavy metals) does  
71 not allow the visualization of the plasma membrane or intracellular compartments at the interface.  
72 In this work, we present a new FIB-SEM method that is capable of *in situ* visualization of the cell-  
73 to-substrate interface with high contrast that resolves subcellular structures and the cell-to-  
74 material junction with 10 nm resolution. The method is compatible with diverse materials (quartz,  
75 doped silicon, conductive polymer) and various surface topographies, allowing clear identification  
76 of how the cell membrane interacts with nanoscale features (protrusions and cracks) on the  
77 substrate.

78 At the core of our FIB-SEM method, there is a new sample preparation method based on  
79 controlled thin-resin plastification of adherent cells with heavy metal staining and as well as  
80 preservation of the contacting material. Unlike the usual hard drying method, this method embeds  
81 cells in a thin plastic layer, which not only preserves the subcellular structures but also provides  
82 a solid support for the subsequent FIB milling. The thin-layer plastification method includes five  
83 major steps: cell fixation, heavy metal staining, resin infiltration, extracellular resin removal, and  
84 resin polymerization (**Figure 1a**). First, mammalian cells cultured on the desired substrate (doped  
85 silicon, polymer or nanostructured quartz) are fixed by glutaraldehyde to crosslink intracellular  
86 structures (*i.e.* proteins) so that they can withstand the subsequent staining and embedding  
87 processes. After fixation, the cells are treated with an osmium series (RO-T-O procedure<sup>21,22</sup>) and  
88 *en bloc* staining (see **Methods**), which not only provide high contrast to membrane and protein  
89 structures, but also help to preserve lipids in subsequent steps. Then, the cells are infiltrated with  
90 liquid epoxy-based resin. Traditional resin embedding procedures for TEM typically result in a 2 -  
91 5 millimeter-thick polymer block, preventing the visualization of the whole-cell morphology. In our  
92 method, after resin infiltration and before resin polymerization, a resin-removal step is introduced  
93 that strips off excess extracellular resin by draining and flushing the sample with ethanol. This  
94 step thins down the resin coating outside the cell membrane to tens of nanometers while  
95 maintaining a stable intracellular resin embedding<sup>20</sup>. The final step involves curing the liquid resin  
96 to a thin layer of plastic with cells embedded inside. Since extracellular resin is largely removed,  
97 cell topography and membrane protrusions in contact with the underlying substrate are clearly  
98 visible under SEM. **Figure 1b** shows a HL-1 cell cultured on a quartz substrate with arrays of  
99 quartz nanopillars, and **Supplementary Figure S1** shows PC12 cells and primary cortical

100 neurons cultured on flat glass substrates, where fine features on the cell membrane are well  
101 preserved.

102 Samples prepared *via* thin layer-plastification are directly mounted on FIB-SEM for *in situ*  
103 examination of the cell-to-substrate interface. For this purpose, we first examine a large sample  
104 area by SEM to identify locations of interest, such as places where cell membranes are in contact  
105 with the surface features like nanopillars. Once a desired area is located, it is coated with a thin  
106 layer of platinum to facilitate the dissipation of ions and prevent sample damage during the next  
107 FIB milling step (see **Methods** and **Supplementary Figure S2**). Then, a high-energy gallium ion  
108 beam is focused on the sample to cut through the platinum protection layer, the cell-embedded  
109 thin plastic layer underneath, and at least 1  $\mu\text{m}$  deep into the substrate. This process is repeated  
110 to remove material and open up a vertical surface (**Figure 1c**). Then, a low-current, e.g. 80 pA,  
111 ion beam is used to remove re-deposited material and polish the cross section. This step is critical  
112 for limiting the curtaining phenomena and ion-induced structural damage at the interface<sup>14</sup>. SEM  
113 visualization of the cross section shows intracellular space and the interface between the cell  
114 membrane and the substrate. Unlike previous FIB-SEM images that usually contain sponge-like  
115 structures with no discernable subcellular structures<sup>15,16,20</sup>, our FIB-SEM image shows very clear  
116 subcellular structures such as the cell membrane, the nucleus, nucleoli, the nuclear envelope,  
117 mitochondria, lysosomes, and multi-vesicular bodies (**Figure 1d**). To be consistent with published  
118 TEM images, all FIB-SEM images are black-and-white inverted. Original images are shown in  
119 **Supplementary Figure S2**.

120 To determine the resolution capabilities of our FIB-SEM method, we have examined a group of  
121 well-characterized cellular compartments using high magnification SEM imaging. **Figure 1e**  
122 shows an image of a mitochondrion that clearly resolves inner and outer membranes (~10 nm  
123 distance) as well as the cristae structures defined by the inner membrane. **Figure 1f** shows the  
124 structure of nuclear envelope with clearly-resolved inner and outer membranes with an interstitial  
125 space of about 20 nm. Endoplasmic reticulum (ER) structures as parallel running membranes can  
126 be seen in the vicinity of the nucleus, and the associated small granules attached to the  
127 membrane of the ER likely are ribosomes (**Supplementary Figure S3a**). Other intracellular  
128 structures have been resolved such as multi-vesicular bodies and endocytic vesicles  
129 (**Supplementary Figure S3b-d**). Furthermore, FIB-SEM clearly reveals that the plasma  
130 membrane is very close (< 50 nm) to the flat substrate surface and contours around local  
131 nanopillar features (**Figure 1g**).

132 Our FIB-SEM method is compatible with substrates with different surface topographies and  
133 different materials, *i.e.* a quartz substrate with nanotubes (**Supplementary Figure S4**). As shown

134 in **Figures 2a, i&ii**, the cell membrane attaches tightly to the flat areas of the quartz substrate  
135 and wraps around the outside surface of a nanotube, with intracellular structures in the vicinity  
136 clearly visible. However, inside the nanotube, the cell membrane did not conformably follow the  
137 surface contour and only extended into the top part of the hollow center (**Figure 2a, iii**) as  
138 previously observed by TEM<sup>23</sup>. In addition to the quartz substrate, we have demonstrated that our  
139 FIB-SEM method can be used for substrates made with the conductive polymer blend Poly(3,4-  
140 ethylenedioxythiophene):Polystyrene Sulfonate (PEDOT:PSS) and doped-silicon (conductive),  
141 with all surface were coated with poly-L-lysine to facilitate cell culture. The surface of the  
142 PEDOT:PSS is patterned into parallel grooves (**Figure 2b, i & Supplementary Figure S4**). The  
143 cell appears well spread on the PEDOT surface, however the FIB-SEM image reveals that the  
144 cell membrane is much further away from the PEDOT substrate (~ 100 nm average on flat areas)  
145 than from the quartz substrate (~25 nm average on flat areas). Locations where the cell  
146 membrane made close contacts with the PEDOT substrate can be clearly identified (arrow heads  
147 in **Figure 2b, ii**). The cell membrane extends into the patterned groove (**Figure 2b, ii**) and into  
148 some local cracks on the substrate (**Figure 2b, iii**). The surface of the doped-silicon substrate  
149 has randomly distributed nanocone features (**Figure 2c, i and Supplementary Figure S4**). By  
150 FIB-SEM, we observed that the cell membrane is far from the flat substrate (~200 nm) in most  
151 places, but makes close contacts with the top of the nanocones.

152 Since FIB-SEM allows repetitive milling and imaging, it is possible to image a volume of interest  
153 (VOI) at high resolution (**Figure 3a**). We used low current (e.g. 80 pA) for sequential FIB milling,  
154 which achieves slice thickness of about 39 nm and well beyond the capability of mechanical slicing  
155 by means of ultramicrotomes (70 - 200 nm). **Figures 3b&c** show two representative cross-  
156 sections of the same cell (shown in **Figure 3a**) interacting with two different lines of nanopillars.  
157 By sequentially imaging a set of 72 sequential sections, we reconstructed a 3D intracellular space  
158 and its interaction with nanopillars using a segmented 3D reconstruction method (**Figure 3d,**  
159 **Supplementary Movie 1**). In particular, we modeled the 3D morphology of the nuclear envelope,  
160 nucleoli, and the non-adherent cellular membrane domain, which were individually constructed  
161 and overlaid to the remaining structures as shown in **Figure 3e**. The nuclear envelope appears  
162 to be bend upward on top of a nanopillar for as much as 800 nm (**Figure 3f**), agreeing well with  
163 our previous observation by TEM<sup>24</sup>.

164 Unlike the ultramicrotome sectioning method that slices materials sequentially in only one  
165 direction, the FIB-SEM method is highly versatile and allows sectioning of the same sample with  
166 different directions at multiple locations. This capability is often important for cells with protrusions  
167 such as neurons. Primary cortical neurons from embryonic rats were cultured on a quartz

168 substrate with arrays of solid nanopillars. After 5 days of culturing *in vitro*, neurons were fixed and  
169 processed for FIB-SEM imaging as described earlier. A SEM image in **Figure 3g (insert)** shows  
170 a neuron cell body together with multiple neurites growing out from the cell body. We first identified  
171 four regions of interest from the SEM image: the cell body, neurite-1, neurite-2 and neurite-3.  
172 Then, after coating a layer of Pt, FIB milling was used to cut open the interfaces along six  
173 connecting lines (yellow arrowed lines corresponding to four regions of interest and green arrowed  
174 lines being the connecting lines in **Figure 3g**). FIB-SEM imaging of the cell body shows the  
175 nuclear, large number of intracellular organelles and the plasma membrane wrapping around  
176 nanopillars (**Figure 3i**). By multiple angle milling, FIB-SEM also offers a unique advantage of  
177 examining a location from multiple directions as shown by the 90-degree intersection between  
178 the neurite-2 and the cell body (**Figure 3h**). The cross-section of neurite-3 is shown in **Figure 2j**,  
179 which illustrates a neurite attached to the top and the side of two nanopillars. A magnified image  
180 of a neurite reveals multiple longitudinally orientated microtubules parallel to the direction of the  
181 neurite (**Figure 3k**), comparable in morphology to those investigated by TEM<sup>25,26</sup>. FIB-SEM  
182 images of Neurite-1 and Neurite-2 connected to the cell body are shown in **Supplementary**  
183 **Figure S5**.

184 Furthermore, we show that our FIB-SEM method is suitable for correlating light and electron  
185 microscopy images (CLEM). For this purpose, we first proved that for cells fixed and stained with  
186 fluorescent phalloidin for actin filaments and immunostained for clathrin (**Supplementary Figure**  
187 **S6**). The fluorescence image taken before the resin infiltration step shows actin accumulation on  
188 nanopillars (**Supplementary Figure S6**), agreeing with results previously reported<sup>24</sup>. Using  
189 nanostructures as location markers, the subsequent resin embedding and SEM imaging shows  
190 the cell morphology perfectly correlating with the fluorescence imaging, which further confirms  
191 that the cell volume was well preserved without any significant alteration.

192 Finally, we demonstrate that our FIB-SEM method is also compatible with correlative microscopy  
193 of living cells transfected with a APEX2-GFP-based construct. Recently, APEX2, a genetically  
194 encoded peroxidase, has been used to selectively enhance the contrast for certain subcellular  
195 structures under TEM<sup>27,28</sup> (e.g. mitochondria). We constructed an APEX2-GFP-CAAX fusion  
196 plasmid that selectively targets APEX2 to the plasma membrane to further enhance the contrast  
197 at the cell-to-material interface. We transfected cells growing on nanopillars with APEX2-GFP-  
198 CAAX allowing initial localization of transfected cells by live fluorescence imaging (**Figure 4a**).  
199 Then, after cell fixation and before osmium staining, 3,3-diaminobenzidine (DAB) and H<sub>2</sub>O<sub>2</sub> are  
200 added to the solution, where APEX2 catalyzes the polymerization and deposition of DAB in its  
201 vicinity. The polyDAB recruits osmium in the subsequent staining step to give greater contrast to

202 APEX2-labeled structures. After thin-resin plastification, the cell can be visualized by SEM  
203 (**Figure 4b**) or ion microscopy (**Supplementary S7**). The FIB milling at the location of interest  
204 opens the cross section for examining the cell-to-substrate interfaces (**Figure 4c**). We compared  
205 the interfaces for APEX2-GFP-CAAX transfected cells vs. non-transfected cells in the same  
206 culture. As shown in **Figures 4d&e**, under identical conditions, APEX2-CAAX transfected cells  
207 show a higher membrane contrast than non-transfected cells (the plasma membrane is visible in  
208 both cases). We note that the APEX2-based contrast enhancement is less distinct than  
209 expected<sup>27</sup>, likely because we used uranyl acetate staining that is known to have a higher affinity  
210 to osmium in membranes than to DAB polymers. Nevertheless, our method uniquely allows direct  
211 correlation between living cells in fluorescence, SEM after thin plastification and the cross section  
212 after selectively FIB milling.

213

214 In conclusion, we demonstrated a new FIB-SEM method for imaging of the cell-to-material  
215 interface *in situ*, without removing the substrate. This method achieves a contrast and resolution  
216 higher than TEM previously used for similar investigations; Moreover, for the first time cells  
217 interfacing materials such as PEDOT:PSS have been investigated besides more common  
218 materials such as quartz and silicon-based surfaces with various topology. Our FIB-SEM method  
219 has unique advantages of examining a large sample area of an artefact-free plastified cell,  
220 opening up cross sections at any desired location, achieving volume reconstruction, performing  
221 multi-directional milling, and compatible with correlative microscopy and APEX2-based  
222 enhancement. In perspective, our method can be used for any cell-material interaction  
223 investigation so that, for example, the interaction of cells/tissue with medical devices.

224

225 **References**

- 226 1. Langer, R. & Tirrell, D. A. Designing materials for biology and medicine. *Nature* **428**, 487–  
227 492 (2004).
- 228 2. Anderson, J. M. Biological Responses to Materials. *Annu. Rev. Mater. Res.* **31**, 81–110  
229 (2001).
- 230 3. Stevens, M. M. & George, J. H. Exploring and Engineering the Cell Surface Interface.  
231 *Science* **310**, 1135–1138 (2005).
- 232 4. Kasemo, B. Biological surface science. *Surf. Sci.* **500**, 656–677 (2002).
- 233 5. Hanson, L., Lin, Z. C., Xie, C., Cui, Y. & Cui, B. Characterization of the Cell-Nanopillar  
234 Interface by Transmission Electron Microscopy. *Nano Lett.* **12**, 5815–5820 (2012).
- 235 6. Wrobel, G. *et al.* Transmission electron microscopy study of the cell–sensor interface. *J. R.*  
236 *Soc. Interface* **5**, 213–222 (2008).
- 237 7. Fendyur, A., Mazurski, N., Shappir, J. & Spira, M. E. Formation of Essential Ultrastructural  
238 Interface between Cultured Hippocampal Cells and Gold Mushroom-Shaped MEA- Toward  
239 ‘IN-CELL’ Recordings from Vertebrate Neurons. *Front. Neuroengineering* **4**, (2011).
- 240 8. Volkert, C. A. & Minor, A. M. Focused Ion Beam Microscopy and Micromachining. *MRS Bull.*  
241 **32**, 389–399 (2007).
- 242 9. Narayan, K. & Subramaniam, S. Focused ion beams in biology. *Nat. Methods* **12**, 1021–  
243 1031 (2015).
- 244 10. Xie, C. *et al.* Noninvasive Neuron Pinning with Nanopillar Arrays. *Nano Lett.* **10**, 4020–4024  
245 (2010).
- 246 11. Xie, C., Lin, Z., Hanson, L., Cui, Y. & Cui, B. Intracellular recording of action potentials by  
247 nanopillar electroporation. *Nat. Nanotechnol.* **7**, 185–190 (2012).
- 248 12. Wierzbicki, R. *et al.* Mapping the Complex Morphology of Cell Interactions with Nanowire  
249 Substrates Using FIB-SEM. *PLoS ONE* **8**, e53307 (2013).



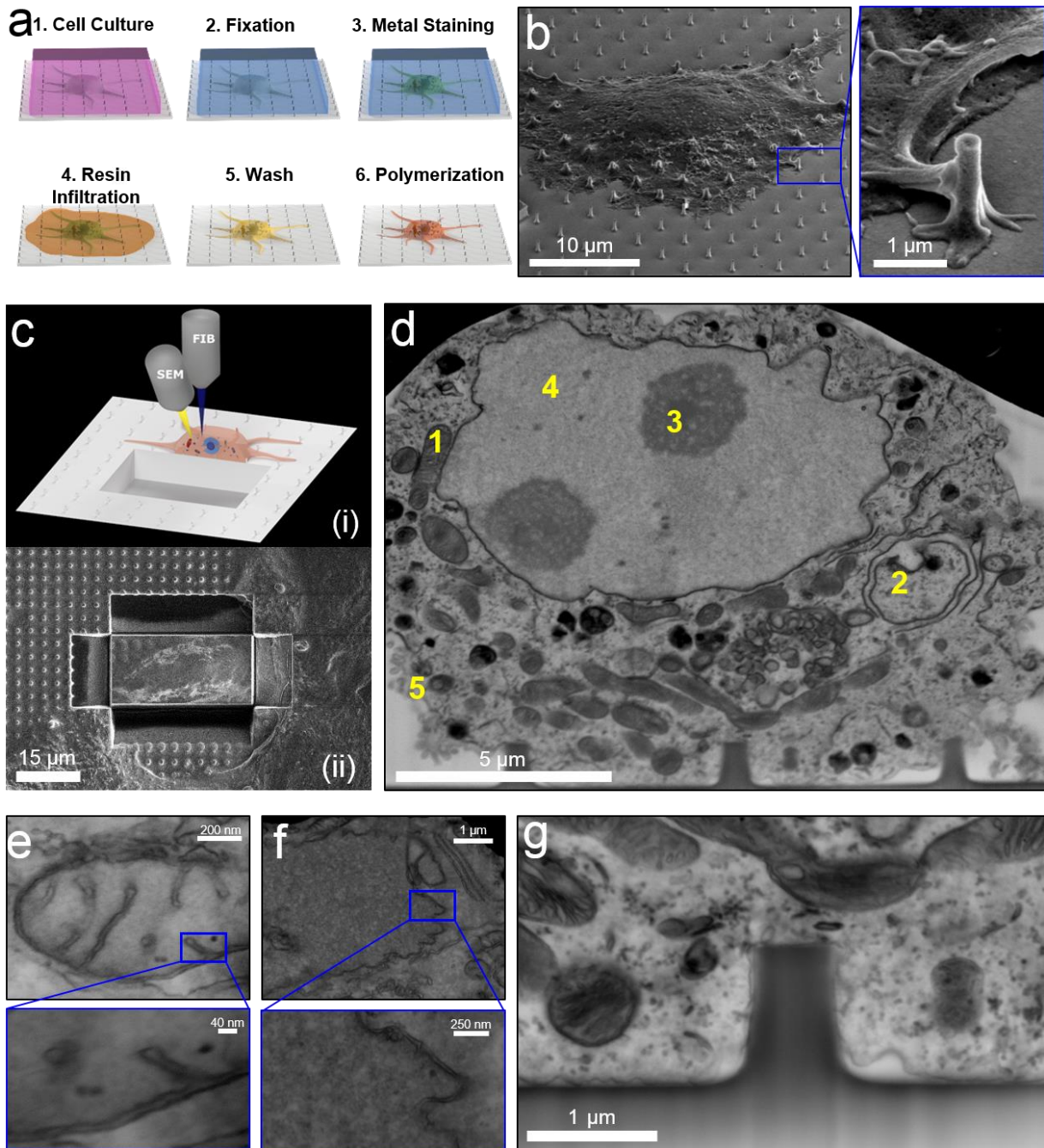
- 250 13. Friedmann, A., Hoess, A., Cismak, A. & Heilmann, A. Investigation of cell–substrate  
251 interactions by focused ion beam preparation and scanning electron microscopy. *Acta*  
252 *Biomater.* **7**, 2499–2507 (2011).
- 253 14. Santoro, F., Neumann, E., Panaitov, G. & Offenhäusser, A. FIB section of cell–electrode  
254 interface: An approach for reducing curtaining effects. *Microelectron. Eng.* **124**, 17–21  
255 (2014).
- 256 15. Santoro, F. *et al.* Interfacing Electrogenic Cells with 3D Nanoelectrodes: Position, Shape,  
257 and Size Matter. *ACS Nano* **8**, 6713–6723 (2014).
- 258 16. Bittermann, A. G., Burkhardt, C. & Hall, H. Imaging of Cell-to-Material Interfaces by SEM  
259 after in situ Focused Ion Beam Milling on Flat Surfaces and Complex 3D-Fibrous Structures.  
260 *Adv. Eng. Mater.* **11**, B182–B188 (2009).
- 261 17. Chiappini, C. *et al.* Biodegradable silicon nanoneedles delivering nucleic acids intracellularly  
262 induce localized in vivo neovascularization. *Nat. Mater.* **14**, 532–539 (2015).
- 263 18. Boyde, A. & MacOnnachie, E. Volume changes during preparation of mouse embryonic  
264 tissue for scanning electron microscopy. *Scanning* **2**, 149–163 (1979).
- 265 19. Gusnard, D. & Kirschner, R. H. Cell and organelle shrinkage during preparation for scanning  
266 electron microscopy: effects of fixation, dehydration and critical point drying. *J. Microsc.* **110**,  
267 51–57 (1977).
- 268 20. Belu, A. *et al.* Ultra-thin resin embedding method for scanning electron microscopy of  
269 individual cells on high and low aspect ratio 3D nanostructures. *J. Microsc.* n/a-n/a (2016).  
270 doi:10.1111/jmi.12378
- 271 21. Tapia, J. C. *et al.* High-contrast en bloc staining of neuronal tissue for field emission  
272 scanning electron microscopy. *Nat. Protoc.* **7**, 193–206 (2012).
- 273 22. Bushby, A. J. *et al.* Imaging three-dimensional tissue architectures by focused ion beam  
274 scanning electron microscopy. *Nat. Protoc.* **6**, 845–858 (2011).

- 275 23. Lin, Z. C., Xie, C., Osakada, Y., Cui, Y. & Cui, B. Iridium oxide nanotube electrodes for  
276 sensitive and prolonged intracellular measurement of action potentials. *Nat. Commun.* **5**,  
277 (2014).
- 278 24. Hanson, L. *et al.* Vertical nanopillars for in situ probing of nuclear mechanics in adherent  
279 cells. *Nat. Nanotechnol.* **10**, 554–562 (2015).
- 280 25. Bartlett, W. P. & Banker, G. A. An electron microscopic study of the development of axons  
281 and dendrites by hippocampal neurons in culture. I. Cells which develop without intercellular  
282 contacts. *J. Neurosci.* **4**, 1944–1953 (1984).
- 283 26. Maxwell, W. L. Damage to Myelin and Oligodendrocytes: A Role in Chronic Outcomes  
284 Following Traumatic Brain Injury? *Brain Sci.* **3**, 1374–1394 (2013).
- 285 27. Lam, S. S. *et al.* Directed evolution of APEX2 for electron microscopy and proximity  
286 labeling. *Nat. Methods* **12**, 51–54 (2015).
- 287 28. Martell, J. D. *et al.* Engineered ascorbate peroxidase as a genetically encoded reporter for  
288 electron microscopy. *Nat. Biotechnol.* **30**, 1143–1148 (2012).

289  
290 **Acknowledgments:** The authors thank the Stanford NanoShared Facility (SNSF) for a seed  
291 grant to a complimentary use of the Helios i600 and Dr. Juliet Jamtgaard and Dr. Richard Chin  
292 for the useful discussions. The authors also acknowledge the National Science Foundation for  
293 the grants NSF 1055112 and NSF 1344302.

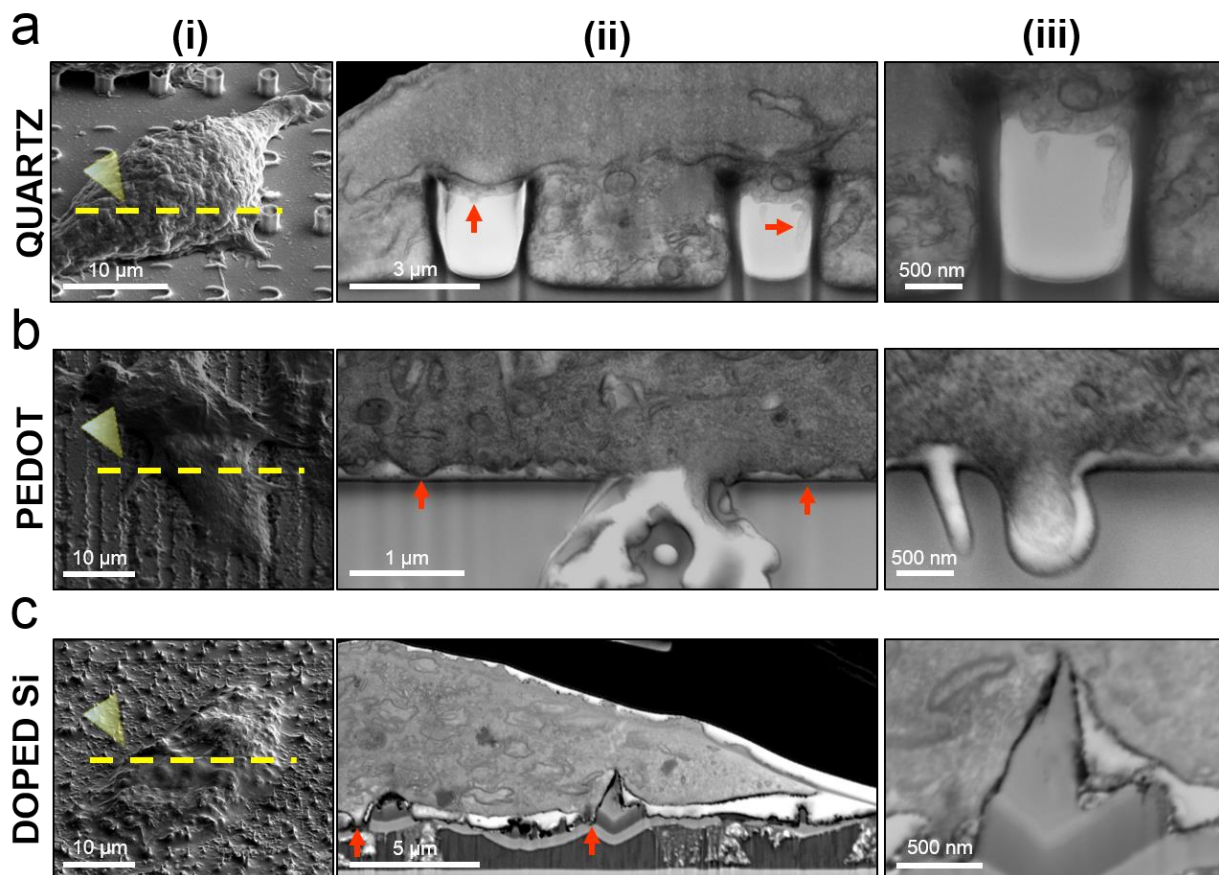
294

295 **Figures' Captions**



296  
297 **Figure 1: Imaging the cell-to-material interface by FIB/SEM.** **a)** Schematics of the sample  
298 preparation procedure by thin-layer resin plastification with contrast enhancement. **b)** A SEM  
299 image of a plastified HL-1 cell on a quartz substrate with nanopillars clearly shows that  
300 extracellular resin is removed and the cell morphology is clearly visible. The insert shows that the  
301 membrane protrusions in contact with a nanopillar are well preserved. **c)** Schematics (i) and

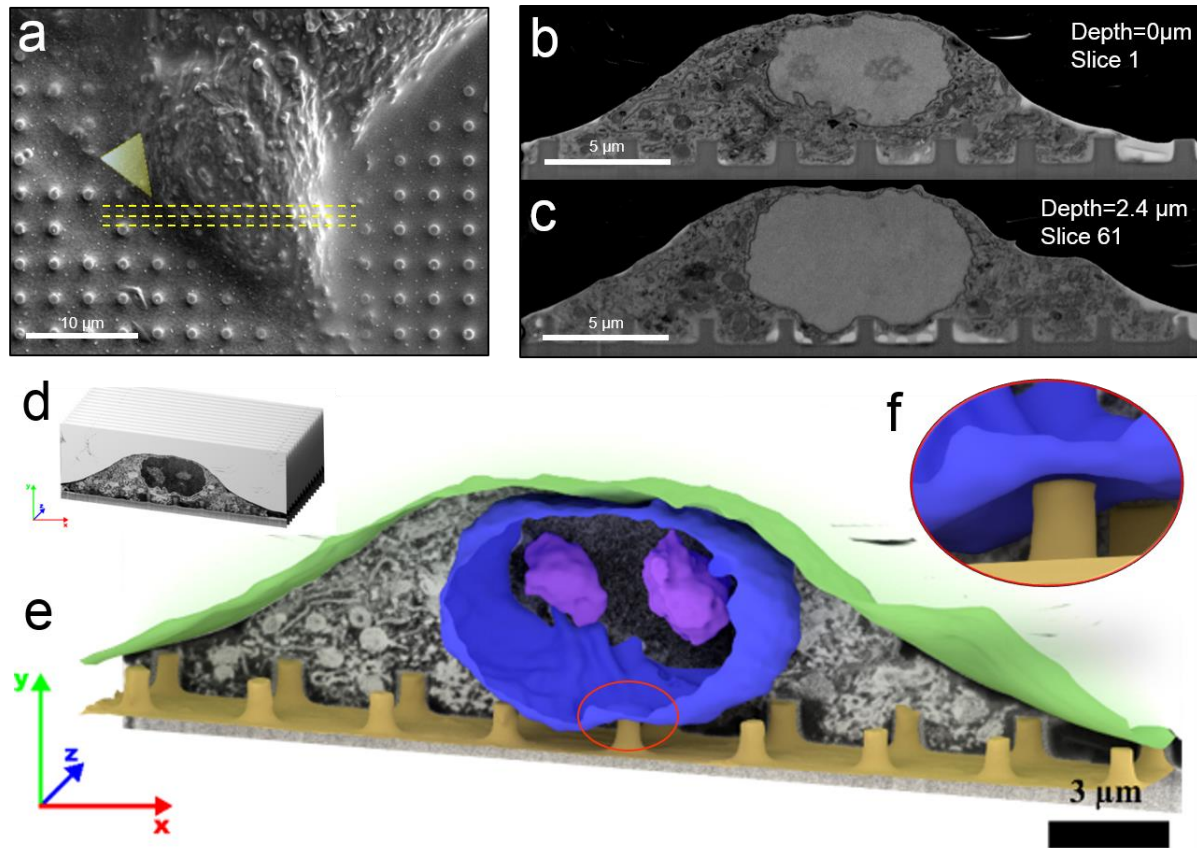
302 experimental results (ii) of using FIB milling to cut trenches through the cell and the substrate and  
303 open up the interface. **d)** A SEM image of the interface after FIB milling reveals intracellular  
304 compartments and organelles such as mitochondria (1), intracellular membranes (2), nucleoli (3),  
305 nucleus (4) and cellular membrane (5). **e-f)** Zoomed-in FIB-SEM images of mitochondria (e) and  
306 nuclear envelope (f), The insets clearly resolves the inner and outer membranes and interstitial  
307 space. **g)** At the interface between the cell and the quartz substrate, the plasma membrane is  
308 shown to warp around a vertical nanopillar. Intracellular structures and local curvatures on the  
309 plasma membrane resembling clathrin-mediated endocytosis events can be clearly identified.  
310 Figures **d-g** have been acquired from backscattered detectors (voltage:5-10 kV, current: 0.64-1.4  
311 nA), tilt is 52°.



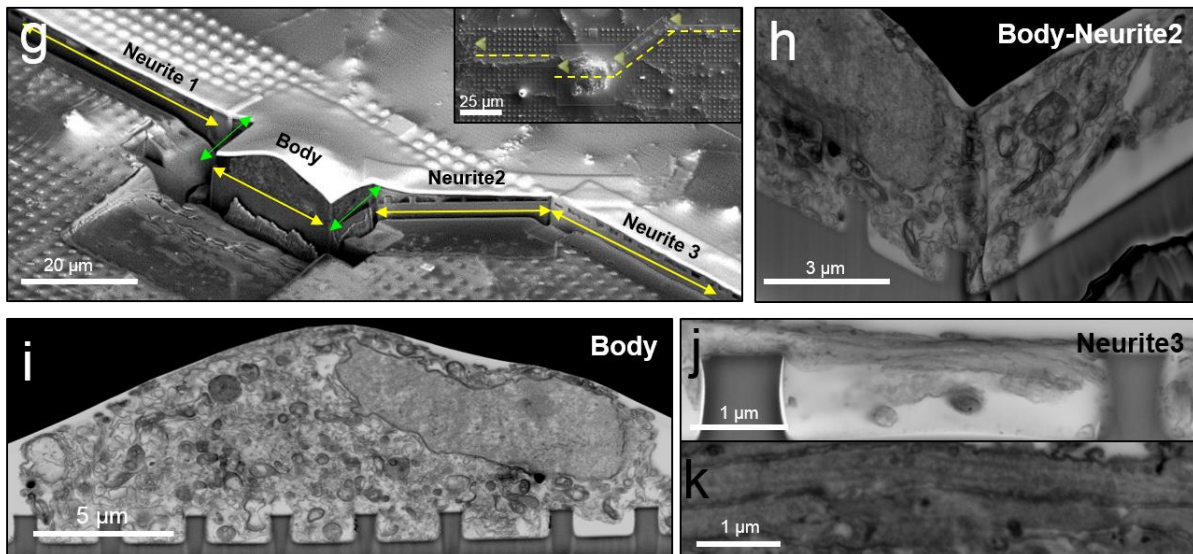
312  
313 **Figure 2: FIB/SEM imaging of the interface is compatible with a variety of materials and**  
314 **surface topography. a)** SEM images of cells cultured on a quartz substrate with nanotubes,  
315 before (i) and after FIB milling (ii, iii). The interface between the cell and the quartz nanotube  
316 shows that the plasma membrane not only warps around the outside of the nanotube and but also  
317 extends into the top part of the nanotube cavity (red arrows and iii). **b)** SEM images of cells  
318 cultured on grooved PEDOT:PSS surface before (i) and after FIB milling (ii); The cell membrane

319 is further away from the PEDOT surface than the quartz surface. Red arrows in (ii) indicate  
320 attachment points of the plasma membrane. Image in (iii) shows the membrane protruding into a  
321 pit on substrate. **c)** SEM images of cells on a doped-silicon substrate with randomly distributed  
322 nanocones before (i) and after FIB milling (ii). Zoom-in image (iii) shows the plasma membrane  
323 partially wraps around the nanocone walls through attachment points (red arrows in ii). Figures  
324 (i) have been acquired by a secondary electron detector, (ii) and (iii) have been acquired with a  
325 backscattered detector (voltage: 5 - 10 kV, current: 0.64 - 1.4 nA). Tilt is 52° in all images.  
326

## SEQUENTIAL MILLING

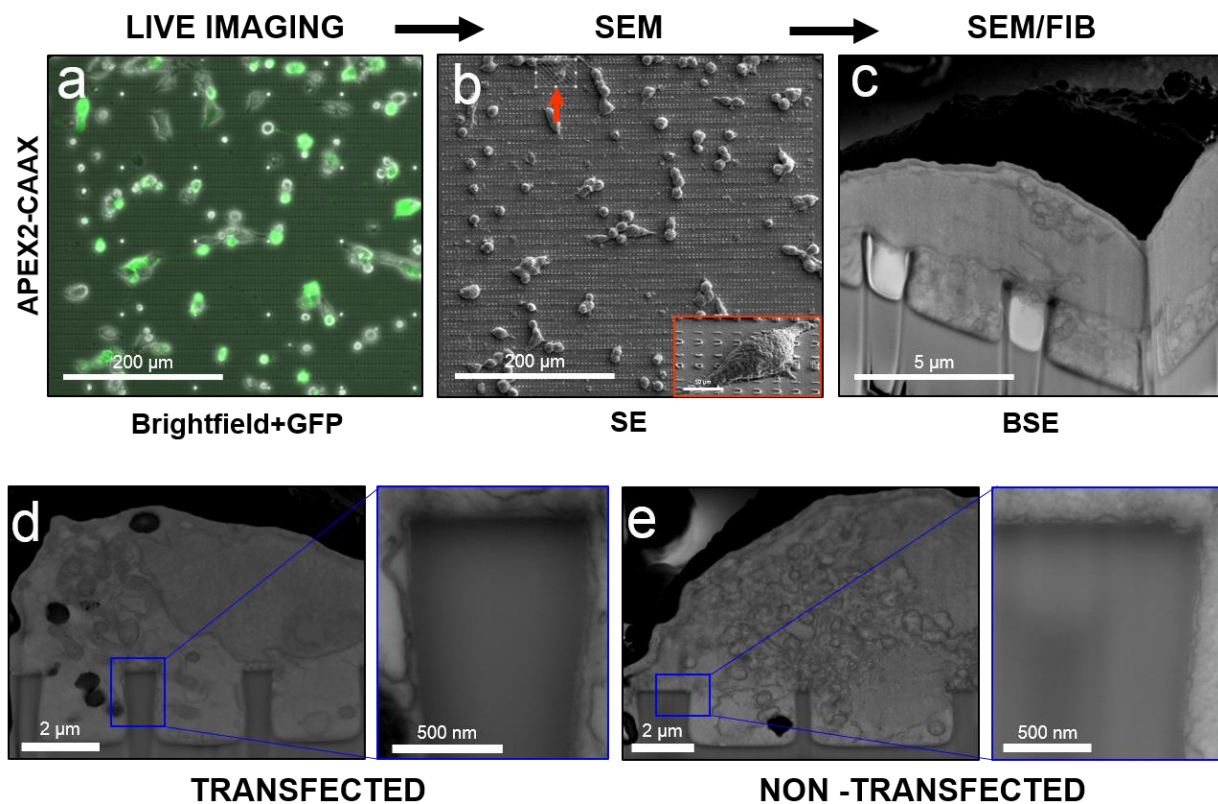


## ANGLED MILLING



327  
328 **Figure 3. FIB-SEM for sequential volumetric imaging and multi-angled imaging. a)** A SEM  
329 image of a plastified HL-1 on nanopillars where yellow dashed lines indicate the region of interest  
330 for the sequential milling. **b-c)** SEM images of two exemplary slices from a stack of 78 slices at

331 two different pillars' lines. **d)** Images collected in the stack were assembled, segmented, and  
332 analyzed. **e)** Automated 3D reconstruction of membrane and nuclear envelope were overlaid to  
333 SEM background image. **f)** Reconstruction shows that the nuclear envelope is deformed upward  
334 by a nanopillar. **g)** FIB milling of a neuron where yellow arrows indicates the regions of interest  
335 and green lines indicates the connecting regions (the inset shows a SEM image of the same  
336 neuron before FIB milling). **h)** A FIB-SEM image of the body-neurite 2 connecting region opened  
337 at 90-degree angle. **i)** A FIB-SEM image of the neuronal body on a line of nanopillars. **j)** A FIB-  
338 SEM image of neurite 3 on top of nanopillars. **k)** Zoomed-in image of neurites reveals multiple  
339 longitudinally orientate microtubules parallel to the direction of the neurite.  
340



341  
342 **Figure 4. Enhancing FIB/SEM imaging by a APEX2 tag.** **a)** Overlay of the brightfield and the  
343 fluorescence (GFP) images of cells transfected with APEX2-GFP-CAAX. **b)** A SEM image of the  
344 same area after thin-layer plastification. The arrow shows the target cell before FIB milling (52°  
345 tilted SEM image in the inset). **c)** The FIB-SEM image of the target cell opened at 90 degree. **d)**  
346 A FIB-SEM image of a APEX2-GFP-CAAX transfected cell. The inset shows the membrane  
347 contrast at the interface. **e)** A FIB-SEM image of a non-transfected cell in the same culture,

348 imaged at the same condition. The inset shows the plasma membrane with lower contrast around  
349 the nanopillar.

350

## 351 **Methods**

### 352 • **Nanostructures fabrication, characterization and preparation.**

#### 353 **Fabrication and characterization of quartz nanopillars.**

354 Nanostructures (NSs) used in this work were fabricated on 4-inch quartz wafer using electron-  
355 beam lithography (EBL). In brief, the wafer was diced into pieces of 2 cm x 2 cm square. After  
356 sonication cleaning in acetone and isopropanol, the pieces were spin-coated with 300 nm of ZEP-  
357 520 (ZEON Chemicals), followed by E-Spacer 300Z (Showa Denko). Desired patterns were  
358 exposed by EBL (Raith150) and developed in xylene. The mask was then created by sputter  
359 deposition of 100 nm Cr and lift-off in acetone. NSs was generated by reactive ion etch with CHF<sub>3</sub>  
360 an O<sub>2</sub> chemistry (AMT 8100 etcher, Applied Materials). Before cell culture, the substrate was  
361 cleaned in O<sub>2</sub> plasma and immersed in Chromium Etchant 1020 (Transene) to remove Cr masks.  
362 SEM (FEI Nova) imaging was performed on 3 nm Cr sputtered substrates to measure the  
363 dimension of different NSs.

#### 364 **Silicon-nanocones**

365 A monolayer polystyrene nanosphere (PS) array, which consists of PSs with an averaged  
366 diameter of 3 μm, were self-assembled on glass-based silicon substrates with a Langmuir–  
367 Blodgett method. To control the effective intervals between the formed silicon nanopillars, a  
368 reactive ion etching (RIE) process with oxygen (O<sub>2</sub>) as an etching gas was then followed to shrink  
369 PSs (with a final diameter of 1 μm). Silicon nanopillars were lastly formed on glass substrates by  
370 introducing chlorine (Cl<sub>2</sub>) and hydrogen bromide (HBr) gasses to reactive-ion-etch the silicon  
371 materials exposed to the plasma.

#### 372 **PEDOT:PSS nanogrooves.**

373 Fused silica glass substrates were cleaned using a standard soap, acetone, isopropanol  
374 sonication sequence. Poly(3,4-ethylenedioxythiophene) polystyrene sulfonate (PEDOT:PSS)  
375 (Heraeus, Clevios PH 1000) solution in water was doped with 5 wt % ethylene glycole, 0.1 wt%  
376 Dodecyl Benzene Sulfonic Acid (DBSA) as a surfactant and 1 wt% (3-  
377 glycidyloxypropyl)trimethoxysilane (GOPTS) as a crosslinking agent to improve film stability. EG,  
378 DBSA and GOPS were all obtained from Sigma Aldrich. After spin-coating at 1000 rpm for 2 mins



379 the films were baked at 120 °C for 10 mins. The nanogrooves were created by focusing a  
380 Ti:Sapphire femtosecond laser (Spectraphysics, 100 fs, 50 mW) to a 5 µm spot right above the  
381 surface of the PEDOT:PSS film and scanning the beam over the films at 2 mm/s.

### 382 **Sample preparation for cell culture.**

383 Quartz substrates were treated with Pirana solution with sulfuric acid and hydrogen peroxide  
384 (Fisher Scientific), in a 7:1 dilution at room temperature overnight. Samples were washed with  
385 distilled water, dried and placed in 70% ethanol in a sterile hood. Samples were washed with  
386 sterile distilled water and allowed to dry. After a 15 mins UV light exposure, samples were  
387 incubated overnight with 0.01% poly-L-lysine (Sigma Life Science) for primary neurons and HEK  
388 cells cultures or with 1 mg/ml fibronectin (Life Technologies) in 0.02% gelatine solution for HL-1  
389 cells. COS-7 cells were directly plated on the substrate after sterilization.

390

### 391 • **Cell culture and transfection**

#### 392 **Primary neurons.**

393 Cortices were extracted from rat embryos at embryonic day 18 and incubated with 0.25% Trypsin/  
394 EDTA (Corning) in 33 mm Petri dish for 5 min at 37°C. The tissue-trypsin/ EDTA solution was  
395 transferred into a 2 mL plastic tube. The tissue settled at the bottom of the tube and left over  
396 trypsin/ EDTA was removed. Neurobasal® media (Gibco) was supplemented with 1% B27  
397 (Gibco), 0.25% glutaMAX, (Gibco) and 0.1% gentamycin antibiotic (Gibco). One ml of warm media  
398 was added and, then, the tube was gently swirled by hand. This procedure was repeated 5 times  
399 and after the last media exchange, the tissue was dissociated until resulting in a cell solution.  
400 80,000 cells were suspended in 3 mL and placed on each substrate. The media was replaced  
401 completely 2 hrs after seeding time. Every second day, half of the media was exchanged with  
402 freshly-prepared warm (supplemented) Neurobasal® media.

#### 403 **HL-1 cells.**

404 Confluent HL-1 cells, cultured in a 33 mm Petri dish, were incubated with 1 mL of 0.25% trypsin/  
405 EDTA for 5 mins at 37° C. The cell-trypsin solution was transferred into a 15 mL tube and 2 mL  
406 of Claycomb media (Sigma Life Science) supplemented with 10% of fetal bovine serum (Sigma-  
407 Aldrich), 100 µg/mL penicillin/streptomycin (Sigma Life Science), 0.1 mM norepinephrine (Sigma-  
408 Aldrich) and 2 mM glutaMAX were add. The cell solution was placed in a centrifuge for 3 mins

409 with a rotation of 1300 rpm. Cells' pellet was resuspended in 1 mL of media and 50  $\mu$ l of the  
410 resuspension was plated on each substrate in addition to 3 mL of supplemented media.

411 **HEK 293 cells.**

412 HEK 293 expressing channels Na<sub>v</sub> 1.3 and K<sub>IR</sub> 2.1 were acquired by Adam Cohen laboratory and  
413 maintained in DMEM/F12 (Gibco), 10% FBS (Gibco), 1% penicillin/streptomycin (100  $\mu$ g/mL,  
414 Gibco), geneticin (500  $\mu$ g/mL, Gibco) and puromycin (2  $\mu$ g/mL, Fisher Scientific). At 80%  
415 confluency, cells were divided, re-suspended and plated on quartz substrates as for HL-1 cells.

416 **COS-7 and U2OS cells.** Cells were maintained in DMEM supplemented with 10% fetal bovine  
417 serum and at 90% confluency they were divided as for HL-1 cells and plated on the substrates.

418

419 • **Ultra-thin plastification and RO-T-O procedure.**

420 Substrates with cells were rinsed with 0.1 M sodium cacodylate buffer (Electron Microscopy  
421 Sciences) and fixed with 3.2% glutaraldehyde (Sigma-Aldrich) at 4°C overnight. Specimens were  
422 then washed (3 x 5 mins) with chilled buffer and quenched with chilled 20 mM glycine solution (20  
423 mins). After rinsing (3x5 mins) with chilled buffer specimens were post-fixed with equal volumes  
424 of 4% osmium tetroxide and 2% potassium ferrocyanide (Electron Microscopy Sciences, *RO* step)  
425 (1 hr on ice). Samples were then washed with chilled buffer (3x 5 mins) and the solution replaced  
426 with freshly prepared 1% thiocarbohydrazide (Electron Microscopy Sciences, *T* step) (20 mins at  
427 room temperature). After rinsing with buffer (2 x 5 mins), the samples were incubated with 2%  
428 aqueous osmium tetroxide (*O* step) (30 mins at room temperature. Cells were again rinsed (2 x 5  
429 mins) with distilled water and then, finally, incubated with syringe-filtered 4% aqueous uranyl  
430 acetate (Electron Microscopy Sciences, *en bloc* step) (overnight 4°C). Cells were rinsed (3 x 5  
431 mins) with chilled distilled water, followed by gradual dehydration in an increasing ethanol series  
432 (10%-30%-50%-70%-90%-100%, 5-10 mins each on ice). The last exchange with 100% ethanol  
433 solution was performed at room temperature. Epoxy-based resin solution was prepared as  
434 previously described(19), and samples infiltrated with increasing concentrations of resin in  
435 100%ethanol, using these ratios: 1:3 (3 hrs), 1:2 (3 hrs),1:1 (overnight), 2:1 (3 hrs), 3:1 (3 hrs).  
436 Infiltration was carried out at room temperature and in a sealed container to prevent evaporation  
437 of ethanol. Samples were then infiltrated with 100% resin overnight at room temperature. The  
438 excess resin removal was carried out by first draining away most of the resin by mounting the  
439 sample vertically for one hour and, then, rapidly rinsing with 100% ethanol prior to polymerization  
440 at 60°C overnight.

441

442 **APEX2 contrast enhancement**

443 **Plasmid preparation.**

444 To make APEX-GFP-CAAX, CIBN-GFP-CAAX (a gift from Dr. Chandra Tucker in University of  
445 Colorado Denver) was first linearized by NheI and AgeI restriction enzymes to remove CIBN.  
446 APEX fragment was amplified from Connexin-GFP-APEX (obtained from Addgene) with forward  
447 primer CGTCAGATCCGCTAGCGCCACCATGGGAAAGTCTTACCCAAGT and reverse  
448 primer CATGGTGGCGACCGGTACATGGGCATCAGCAAACCCAAGC. Using InFusion cloning  
449 kit (Clontech, Mountain View, CA, USA), APEX was inserted into the  
450 previously linearized backbone.

451 **Transfection.**

452 Cells were transfected with APEX2-GFP-CAAX plasmids (340 ng) using Lipofectamine 2000 (Life  
453 Technologies) according to the manufacturer's protocol. The transfected cells were allowed to  
454 recover and express the desired protein for 18 hrs prior to live imaging performed with a  
455 microscope LEICA DMI 6000B (Leica).

456 **Osmication and staining.**

457 Cells were washed with 0.1 M sodium cacodylate buffer and fixed with 2.5% glutaraldehyde for  
458 at least 1 hr at 4°C. Substrates were washed three times with chilled buffer and quenched with  
459 chilled 20 mM glycine in buffer solution for 20 mins. Afterwards, cells were washed with chilled  
460 buffer followed by 3,3'-diaminobenzidine (Sigma-Aldrich) solution which had been freshly  
461 prepared as follows: DAB powder was mixed with 1 M HCl to reach a final concentration of 1.4  
462 mM. Thereafter the DAB solution was mixed (equal volumes) to 0.03% H<sub>2</sub>O<sub>2</sub> (in 0.1 M cacodylate  
463 buffer). Cells were osmicated with 2% osmium tetroxide for 1 hr at 4°C, washed with chilled buffer  
464 and incubated with 2% potassium ferrocyanide overnight at 4°C for the reduced osmium procedure.  
465 For membrane enhancement in FIB-SEM, cells were treated with RO-T-O enhancement, ethanol  
466 dehydration and ultra-thin plastification as described above.

467

468 • **Scanning electron microscopy imaging and focused ion beam sectioning**

469 **Sample preparation.**

470 Each sample was glued with colloidal silver paste (Ted Pella Inc.) to a standard stub 18 mm pin  
471 mount (Ted Pella Inc.). A very thin layer of gold-palladium alloy was sputtered on the sample  
472 before imaging.

### 473 **SEM imaging.**

474 Samples were loaded into the vacuum chamber of a dual-beam Helios Nanolab600i FIB-SEM  
475 (FEI). For selecting a region of interest, an (electron) beam with accelerating voltage 3-5 kV, and  
476 current 21 pA - 1.4 nA, was applied. For image acquisition of whole cells (*i.e.* Figure 1b) a  
477 secondary electrons detector was used. For cross section imaging, a beam acceleration voltage  
478 of 2 kV - 10 kV was selected, with the current ranging between 0.17 - 1.4 nA, while using a  
479 backscattered electrons detector (immersion mode, dynamic focus disabled in cross section,  
480 stage bias zero), a dwell time of 100  $\mu$ s and 3072 x 2048 pixel store resolution. For the sequential  
481 sectioning, the function iSPI was enabled in order to slice and acquire an image of the stack every  
482 38.5 nm with 5 kV voltage, 1.4 nA current and 1024x884 resolution.

### 483 **FIB sectioning.**

484 Regions of interest were preserved by electron-assisted deposition of a 0.5  $\mu$ m double platinum  
485 layer, and ion-assisted deposition of a (nominal) 1 $\mu$ m thick coating. First, trenches were created  
486 with an etching procedure fixing an acceleration voltage of 30 kV and currents in the range 9.1  
487 nA – 0.74 nA depending on the effective area to remove. A fine polishing procedure of the  
488 resulting cross sections was carried out on the sections, with a voltage of 30 kV and lower currents  
489 in the range 0.74 nA - 80 pA so that re-deposition phenomena in the cross section are very limited.

### 490 **Image analysis and 3D reconstruction.**

491 All images were pre-processed with ImageJ (National Institute of Health, USA,  
492 <http://imagej.nih.gov/ij>). The images of the sequential cross sections shown in Figure 2, were  
493 collected as a stack, analyzed and processed with an open source tool chain based on Python  
494 (Python Software Foundation, USA, <http://www.python.org>) scripts and tools. The image stack  
495 was cropped, filtered and down-sampled. The isotropic resolution in x, y and z amounts to 38.5  
496 nm. The reconstructed data are visualized with Blender. (Blender Foundation, Netherlands,  
497 <http://www.blender.org>).

498

499

500